Reciprocal Relation Between Intraband Carrier Generation and Interband Recombination at the Heterointerface of Two-Step Photon Up-Conversion Solar Cells

Noriyuki Kinugawa, Shigeo Asahi,* and Takashi Kita

Department of Electrical and Electronic Engineering, Graduate School of Engineering, Kobe University, 1-1 Rokkodai, Nada, Kobe 657-8501, Japan

(Received 21 December 2019; revised 19 February 2020; accepted 1 June 2020; published 6 July 2020)

Photon up-conversion processes are considered beneficial for energy-conversion devices. The recently proposed two-step photon up-conversion (TPU) solar-cell design employs an intermediate level with a high electron occupation probability. To understand the device physics, a quantitative evaluation of the different current-generation and loss mechanisms is required. In the present work, we use a TPU solar cell containing an InAs/GaAs quantum-dot layer located 10 nm in front of an $Al_{0.3}Ga_{0.7}As$/GaAs heterointerface. We study the relation between the photocurrent (PC), radiative recombination, and nonradiative recombination as a function of the bias voltage. The radiative interband recombination is evaluated by integrating the photoluminescence (PL) over the range from 1000 to 1300 nm. The magnitudes of the PC and PL signals generated via interband excitation of the GaAs layer depend on the bias voltage; a higher forward bias reduces the PC and increases the PL intensity. We verify that, under additional infrared light illumination at 1319 nm, which induces intraband transitions, the PC density increases while the PL intensity significantly decreases. This PC enhancement exhibits a maximum at −0.6 V, which reflects the optimum internal electric field strength for maximizing the TPU efficiency.

DOI: 10.1103/PhysRevApplied.14.014010

I. INTRODUCTION

The realization and large-scale implementation of solar cells (SCs) with high conversion efficiencies is expected to play an important role in resolving global energy and environmental issues [1–7]. The conventional single-junction SC design implies unavoidable losses such as thermalization losses (via hot-carrier relaxation) and transmission losses [8]. Consequently, the theoretical upper limit of the conversion efficiency of a single-junction SC is well below unity: 33% under 1 sun and 41% under maximum sunlight concentration [8–10]. To surpass this fundamental limitation of the single-junction SC, improved device concepts that allow us to significantly reduce the transmission (thermalization) loss by harvesting low-energy (high-energy) photons in solar radiation have to be considered [8]. While the multijunction solar-cell design achieves significantly higher efficiencies [7], the loss caused by transmission of sub-band-gap photons is still present. In 1997, it was shown that additional absorption via an intermediate level located in the energy gap between the conduction band (CB) and the valence band (VB) of a semiconductor can lead to a high conversion efficiency owing to a higher photocurrent (PC) [11]. The theoretical conversion efficiency calculated in the framework of the detailed-balanced model for an ideal single-junction SC including one intermediate band (IB) is 47% under 1 sun and 63% under maximum sunlight concentration [10,11]. These high efficiencies are a result of considering an efficient two-step photon up-conversion (TPU) process; by absorbing a sub-band-gap photon, which would be transmitted in the case of a conventional SC, an electron is pumped from the VB to the IB, and upon absorbing another sub-band-gap photon, the electron is pumped to the CB [12].

To obtain an efficient intraband transition from the IB to the CB in a SC exposed to sunlight, the IB is usually implemented in the form of a three-dimensionally confined system such as one composed of quantum dots (QDs) or impurities [13–17]. QDs have been widely used because their growth is highly controllable [18–20]. However, electrons that have been excited to the CB (via either TPU or direct excitation) relax easily to the IB and then quickly recombine with holes in the VB. This relaxation results in low effective TPU efficiencies and gives rise to a drop in the output voltage [6,21]. Moreover, a relatively strong intraband transition is essential in order to approach the ideal conversion efficiency [22], but this requires a long electron lifetime in the IB [6,23]. New design concepts may enable the realization of higher TPU efficiencies.

We have recently proposed a so-called TPU-SC, which utilizes a heterointerface comprising a wide-gap

*asahis@people.kobe-u.ac.jp

semiconductor (WGS) and a narrow-gap semiconductor (NGS) in the intrinsic region of an *n-i-p* junction [24–26]. Here, electrons that have been photogenerated (via direct excitation) in the NGS drift toward the heterointerface and accumulate due to the potential barrier formed by the CB offset. As the electrons are spatially separated from the photogenerated holes by the internal electric field, this design achieves a long electron lifetime. In this device, the electrons accumulated at the interface are transferred to the CB of the $Al_{0.3}Ga_{0.7}As$ barrier as a result of two factors: intraband transitions induced by absorption of infrared (IR) photons, and drift due to the electric field at the interface. We note that QDs are important for relaxation of the optical selection rule for the intraband transition [27,28], and we have demonstrated a remarkable IR-induced enhancement of the PC and of the open-circuit voltage in a TPU-SC with an InAs/GaAs QD layer immediately in front of an $Al_{0.3}Ga_{0.7}As$/GaAs heterointerface [24,25]. For further development of the TPU-SC, a detailed analysis of the connections between the different carrier extraction mechanisms and recombination mechanisms at the heterointerface during device operation is indispensable.

In the work presented here, we investigate the PC generated by the TPU process and the photoluminescence (PL) at the $Al_{0.3}Ga_{0.7}As$/GaAs heterointerface of a TPU-SC device with a QD layer near the heterointerface. The data are measured as a function of the bias voltage, and we discuss the efficiencies of carrier collection, radiative recombination, and nonradiative recombination. The PC density increases under additional IR illumination, and, at the same time, the total PL intensity in the range from 1000 to 1300 nm decreases. This observation reveals a reciprocal relation between the intraband transition and interband recombination. A detailed analysis of the results elucidates how the carrier collection efficiency depends on the bias voltage and IR illumination.

II. EXPERIMENT

A. Structure of the TPU-SC device

The TPU-SC used in this study is grown on a p^+-GaAs(001) substrate by solid-source molecular-beam epitaxy. The TPU-SC comprises an *n-i-p* junction structure, where the central intrinsic part is an $Al_{0.3}Ga_{0.7}As$/GaAs heterostructure with an InAs/GaAs QD layer located 10 nm in front of the heterointerface. Figure 1 shows the band structure of the TPU-SC, obtained by a theoretical simulation without considering the InAs QDs [29]. The CB and VB offsets at the heterointerface are 0.23 and 0.17 eV, respectively. The estimated electric field in the *i* layer is 10.5 kV/cm.

First, a 150-nm-thick *p*-GaAs (Be 2.0×10^{19} /cm^3) layer is grown on a 400-nm-thick p^+-GaAs (Be 1.0×10^{19} /cm^3)

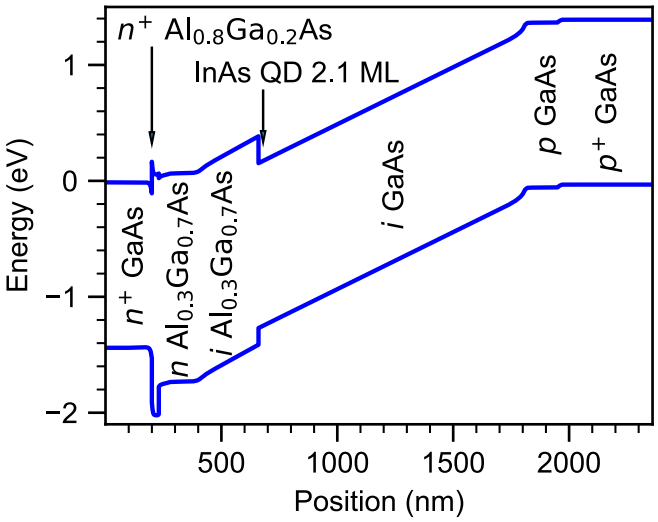

FIG. 1. Band diagram calculated for a TPU-SC without InAs QDs for a bias voltage of 0 V. In the actual SC device, an InAs/GaAs QD layer with a thickness equivalent to 2.1 monolayers (ML) is inserted 10 nm in front of the heterointerface.

buffer layer at a substrate temperature of 550 °C. Subsequently, a 1400-nm-thick intrinsic region is fabricated, which comprises a 1140-nm-thick NGS region based on GaAs, an InAs QD layer, a GaAs capping layer with a thickness of 10 nm, and a WGS region ($Al_{0.3}Ga_{0.7}As$, 250 nm). The nominal thickness of the InAs layer is 0.64 nm (2.1 monolayers). The typical height and width of the QDs, formed by the Stranski-Krastanov growth mode, are 3 and 20 nm, respectively, and the QD density is approximately 1.0×10^{10} /cm^2 [18]. The substrate temperature before the growth of the InAs QDs is 550 °C. The InAs QDs and the GaAs capping layer are grown at 490 °C. On top of this intrinsic structure, an *n*-$Al_{0.3}Ga_{0.7}As$ (Si 1.0×10^{17} /cm^3) layer, an n^+-$Al_{0.3}Ga_{0.7}As$ (Si 2.5×10^{17} /cm^3) layer, an n^+-$Al_{0.8}Ga_{0.2}As$ (Si 2.5×10^{18} /cm^3) window layer, and a final 200-nm-thick n^+-GaAs (Si: 2.5×10^{18} /cm^3) layer are grown. The beam-equivalent pressures of the As_2 flux during the GaAs and (AlGa)As growth sequences is 1.5×10^{-3} Pa. For the current measurements, metal Au/Au-Ge and Au/Au-Zn electrodes are deposited on the top and bottom surfaces, respectively. Finally, the n^+-GaAs layer on the surface is removed by etching except for the electrode region.

B. External quantum efficiency (EQE)

Measurements of the EQE are performed under short-circuit conditions at room temperature. For the excitation, white light generated by a tungsten halogen lamp is passed through a 140-mm single monochromator and modulated at 800 Hz by an optical chopper. The integrated power density of the excitation beam obtained is approximately 2 mW/cm^2 and exhibits a wavelength dependence. The PC

is detected by a current amplifier and a lock-in amplifier synchronized with the optical chopper. We also measure the change in the EQE induced by additional irradiation with IR light (the EQE and the change in the EQE are denoted hereafter by η_Q and $\Delta\eta_Q$, respectively). The IR light is generated by a continuous-wave laser diode (LD) with a wavelength of 1300 nm. The excitation power density of the 1300-nm IR light is 170 mW/cm^2.

C. Simultaneous measurements of PC and PL at various bias voltages

To investigate the details of the carrier collection and recombination processes occurring at the heterointerface, we perform simultaneous measurements of the total PC and the total PL intensity in the wavelength region from 1000 to 1300 nm under bias conditions ranging from −2 to 1 V. This wavelength region covers the PL from InAs QDs. The radiative recombination process occurs dominantly in the InAs QDs. Here, we use two lasers: a continuous-wave LD with a wavelength of 784 nm (1.58 eV) for the interband excitation and a solid-state laser with a wavelength of 1319 nm (0.94 eV) for the intraband excitation (excitation to the $Al_{0.3}Ga_{0.7}As$ CB). Each type of excitation light is guided to the TPU-SC by an optical fiber. The excitation power densities for the interband and intraband excitation are 0.70 and 1.85 W/cm^2, respectively. The PL signal emitted from the TPU-SC is first dispersed by a single monochromator and then detected by an (InGa)As diode array. The PC is detected by a source meter (Keithley). All measurements are conducted at room temperature.

III. RESULTS AND DISCUSSION

A. External-quantum-efficiency spectra

Figures 2(a) and 2(b) show the spectra of the EQE, η_Q, and its change, $\Delta\eta_Q$, respectively, under short-circuit conditions. The blue curve in Fig. 2(a) is obtained without additional IR irradiation. Two clear absorption edges appear at 685 and 875 nm, which correspond to the band gaps of $Al_{0.3}Ga_{0.7}As$ and GaAs, respectively. The feature at 915 nm is assigned to the InAs wetting layer. When the $Al_{0.3}Ga_{0.7}As$ layer is directly excited, the photogenerated electrons and holes drift in opposite directions and are collected at the corresponding electrodes. On the other hand, photons with wavelengths longer than 685 nm pass through the $Al_{0.3}Ga_{0.7}As$ and can generate carriers in the GaAs via interband excitation (if the photon energy is sufficiently high). Because these directly excited electrons are partially blocked by the $Al_{0.3}Ga_{0.7}As$ barrier at the heterointerface, a drop in the η_Q signal is observed in Fig. 2(a) for wavelengths larger than 685 nm. The red line in Fig. 2(a) shows the curve obtained with additional IR irradiation at 1300 nm. This IR light cannot cause any interband transitions, as the photon energy is lower than the lowest interband transition energy (that is, the lowest excited state of an InAs QD, at approximately 1.05 eV). Instead, the additional IR light pumps electrons at the heterointerface above the $Al_{0.3}Ga_{0.7}As$ barrier via an intraband excitation process, and therefore the absorption edge at 685 nm disappears. This is a typical feature of the TPU-SC; electrons that have accumulated at the heterointerface and reached a high density are efficiently pumped above the barrier by absorbing low-energy photons. The efficiency of this process is confirmed in Fig. 2(b): the value of $\Delta\eta_Q$ in the wavelength range from 700 to 860 nm is approximately 15%. Note that this value is smaller than the approximately 30% reported in our previous work [24]. This is explained by the fact that the magnitude of $\Delta\eta_Q$ depends strongly on the excitation power density used to induce the interband transitions [24], that is, $\Delta\eta_Q$ decreases significantly as the excitation power density increases.

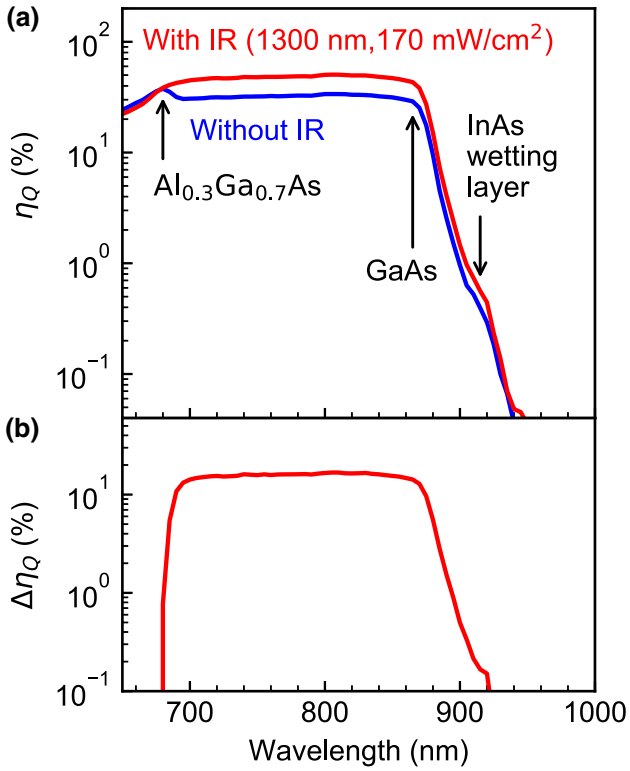

FIG. 2. (a) Room-temperature EQE spectra (η_Q) under short-circuit conditions with and without additional IR irradiation (1300 nm), shown by red and blue curves, respectively. (b) Change in EQE spectrum ($\Delta\eta_Q$) obtained by subtracting the blue curve in (a) from the red curve in (a).

B. Bias-voltage dependence of PC and PL

Figure 3 shows PL spectra measured under short-circuit conditions. Here, interband transitions are induced by the

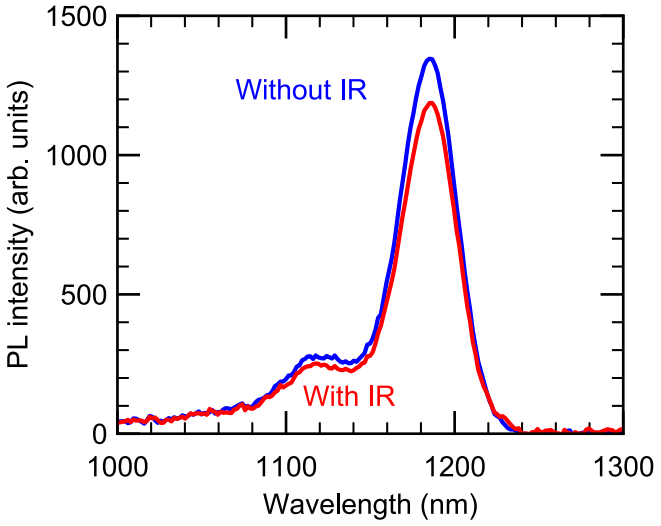

FIG. 3. Room-temperature PL spectra obtained from the device under short-circuit conditions. The blue curve is obtained under excitation with 748-nm light, and the red curve under simultaneous excitation with 748-nm light and IR light at 1319 nm.

784-nm light. The red and blue curves indicate the spectra obtained with and without the additional IR irradiation (at 1319 nm), respectively. As the $Al_{0.3}Ga_{0.7}As$ layers are transparent to the 784-nm light, this light directly excites the GaAs. The electrons generated in the GaAs drift toward the *n*-layer side, but are partially blocked by the $Al_{0.3}Ga_{0.7}As$ barrier and can induce PL in the QDs after the electrons have relaxed from the GaAs CB to QD states. The PL peak at 1185 nm and the small sideband peak at 1120 nm correspond to the lowest excited state and the second lowest excited state, respectively, in the InAs QDs. When the additional IR light irradiates the TPU-SC, the PL intensity decreases obviously, indicating that the IR light activates electrons from these InAs QD levels. As the IR photon energy is larger than the energy offset with respect to the upper CB edge of the barrier, the electron density at the heterointerface decreases as a result of carrier activation and extraction via the internal electric field. The influence of the electric field is evaluated in the following.

Figure 4(a) compares the bias-voltage dependences of the PC density and the PL intensity integrated from 1000 to 1300 nm, which corresponds to the region containing confined states in the InAs layer. The internal electric field increases as the bias voltage becomes more negative, resulting in a large PC density and a low PL intensity at a reverse bias of −2 V. In the forward-bias region, the PC exhibits a remarkable decrease at voltages above 0.58 V. Here, the carrier recombination rate at the heterointerface is very high, and also the PL intensity increases dramatically. This is the typical reciprocal relation observed between PC and PL [30–35]. Furthermore, by comparing the red and blue curves in Fig. 4(a), we find that, for all

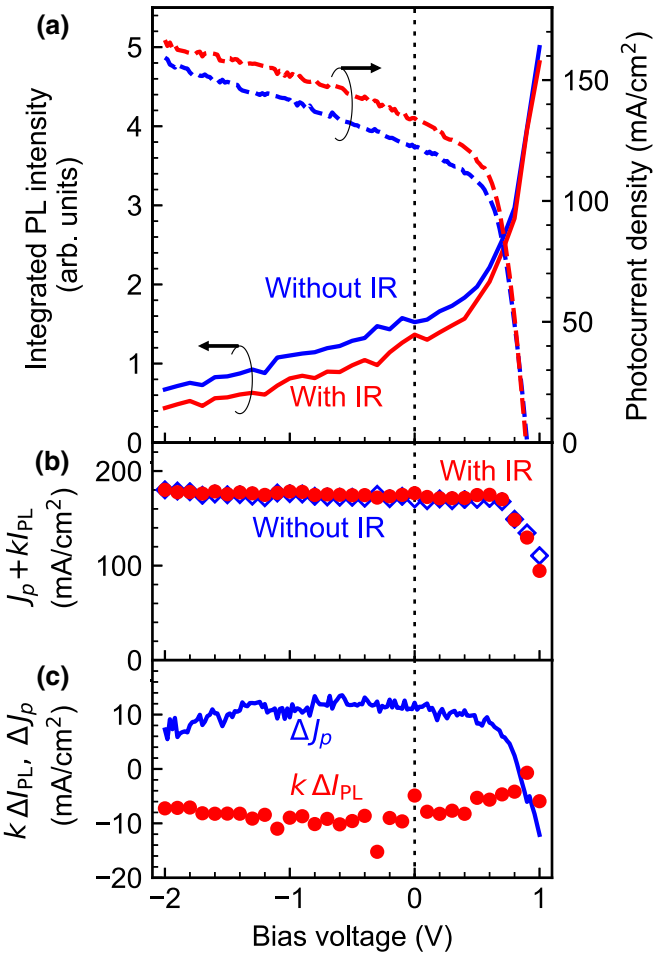

FIG. 4. (a) Integrated PL intensity (integration range 1000–1300 nm) and PC density as a function of the bias voltage. The red curves represent data obtained using 784-nm light and IR light at 1319 nm. The blue curves indicate the case of irradiation with 784-nm light only. (b) Bias-voltage dependences of $J_p + kI_{PL}$ measured with and without IR irradiation. J_p and kI_{PL} are the PC density and the evaluated radiative-recombination current density, respectively. (c) Bias-voltage dependences of the change in the radiative-recombination current density, $k\,\Delta I_{PL}$, and the increase in the PC density caused by TPU, ΔJ_p.

voltages, the PC increases when the additional IR illumination is applied, while the radiative recombination rate decreases as a result of the above-mentioned lower electron density at the interface.

C. Reciprocal relation between PC and PL

The correlation of the PC and the PL intensity in the case of interband excitation via 784-nm light is discussed using the following equation:

$$q\dot{N}_{in} = J_p(V) + R_{rad}(V) + R_{nr}(V), \tag{1}$$

where $\dot{N}_{in}$ is the absorbed photon flux per unit cross section, q is the elementary charge, $J_p(V)$ is the PC

density as a function of the bias voltage V (the dark current is not contained in this term), $R_{\rm rad}(V)$ is the radiative-recombination current density, and $R_{\rm nr}(V)$ is the nonradiative-recombination current density. The terms $J_p(V)$, $R_{\rm rad}(V)$, and $R_{\rm nr}(V)$ are expressed in units of charge current per area, e.g., mA/cm^2. Here, we introduce a voltage-independent proportionality factor k that allows us to express $R_{\rm rad}(V)$ in Eq. (1) in terms of the PL intensity: $R_{\rm rad}(V) = kI_{\rm PL}(V)$, where $I_{\rm PL}(V)$ is the voltage-dependent integrated PL intensity shown in Fig. 4(a). Obviously, $J_p(V) + kI_{\rm PL}(V) + R_{\rm nr}(V)$ is constant as long as the excitation density is not changed. In Eq. (1), we use a value of $q\dot{N}_{\rm in}$ of 190 mA/cm^2, which is calculated by using the excitation power density, the photoreflection of 784-nm light at the SC surface, the absorption coefficient of GaAs (the NGS), and the thickness of the NGS layer. Furthermore, Eq. (1) holds even in the case of additional IR irradiation, because the IR light does not affect $N_{\rm in}$. If we assume that all electrons that have been excited by the IR light are collected at a bias of -2 V, then the IR-induced change in the PC at -2 V, $\Delta J_p(-2\ {\rm V})$, equals the IR-induced change in the PL intensity, $k\,\Delta I_{\rm PL}(-2\ {\rm V})$. Here, we assume that the IR irradiation does not change $R_{\rm nr}(-2\ {\rm V})$, because of the strong electric field of approximately 24 kV/cm. Thus, we can evaluate k and calculate $J_p(V) + kI_{\rm PL}(V)$ at other bias voltages. The results are shown in Fig. 4(b). We find that the values of $J_p + kI_{\rm PL}$ observed with and without IR irradiation coincide over the whole measurement range. Starting from -2 V, $J_p + kI_{\rm PL}$ decreases only slightly as the bias voltage becomes more positive up to 0.58 V, according to the well-known behavior of a p-n junction [10], and then exhibits a rapid decrease according to the bias dependence of the nonradiative recombination rate. The slight decrease in $J_p + kI_{\rm PL}$ is caused by an increase in $R_{\rm nr}(V)$. Conversely, an IR-induced change in $R_{\rm nr}(V)$ is not confirmed, because $J_p + kI_{\rm PL}$ is not affected by the IR irradiation.

Figure 4(c) shows the bias-voltage dependences of ΔJ_p and $k\,\Delta I_{\rm PL}$. Near a bias voltage of -0.6 V, ΔJ_p exhibits a gentle peak, which is considered to be a result of the trade-off relationship between extraction of carriers after TPU (by the electric field) and tunneling of carriers at the heterointerface: while a higher internal electric field facilitates extraction of electrons excited by the additional IR light (leading to an increase in ΔJ_p), a very strong electric field also induces tunneling at the heterointerface. The latter process reduces the electron density at the heterointerface independently of the IR light, and thus reduces ΔJ_p. While ΔJ_p exhibits a gentle peak near -0.6 V, the $k\,\Delta I_{\rm PL}$ signal exhibits a corresponding gentle dip. Note that $I_{\rm PL}$ exhibits a monotonic increase in the same bias-voltage region in Fig. 4(a). The different behaviors of $I_{\rm PL}$ and $\Delta I_{\rm PL}$ are attributed to the fact that $I_{\rm PL}$ is affected by both the electron and the hole densities, while $\Delta I_{\rm PL}$ is affected only by the electron density, as explained in the following. In general, the PL intensity of an InAs QD is proportional to the product of the electron and hole densities in the QD. In the TPU-SC, the occupation probabilities of the lowest excited states in the InAs QDs are very high due to the electron barrier at the heterointerface, even under forward-bias conditions. On the other hand, the hole density in the InAs QDs is strongly affected by the bias voltage. Therefore, the bias-voltage dependence of $\Delta I_{\rm PL}$, which reflects the change in the electron density upon IR illumination, is less pronounced than that of $I_{\rm PL}$.

D. Evaluation of absolute carrier collection efficiency

Figures 5(a) and 5(b) summarize the ratios of the different types of current loss (radiative and nonradiative recombination) and carrier extraction mechanisms (TPU, thermal activation, and tunneling) with and without the additional IR irradiation. The purple area indicates the fraction corresponding to thermal escape and tunneling. Therefore, the carrier collection efficiency of the device without IR irradiation follows the border between the purple and green areas in Fig. 5(a). The blue area in Fig. 5(b) corresponds to the PC enhancement caused by TPU [ΔJ_p in Fig. 4(c)]. Hence, the carrier collection efficiency of the device under additional IR illumination follows the border between the blue and green areas. The green and orange areas indicate the radiative and nonradiative recombination, respectively. Here, the internal quantum efficiency, given by the ratio of $R_{\rm rad}(0\ {\rm V})$ to the sum of $R_{\rm rad}(0\ {\rm V})$, $R_{\rm nr}(0\ {\rm V})$, and $J_p(0\ {\rm V})$, is 25%. This value is higher than the efficiency of 8.8% estimated from the temperature dependence of the PL intensity shown in Fig. 4 of Ref. [24]. The difference is caused by the excitation intensity. The excitation power density in Fig. 4 of Ref. [24] was 2.1 mW/cm^2, while that in the present study is 700 mW/cm^2. It is noted that the nonradiative component is overestimated because we do not take into account the weak PL from the InAs wetting layer and the GaAs in our analysis. Within the accuracy of our assumptions, we find that 7% of the photogenerated carriers in the GaAs are collected via TPU in our device at -0.6 V. As ΔJ_p is generated by adiabatic excitation in the TPU process, it is expected that the output voltage will be boosted [36]. Figure 5(c) compares the voltage increase ΔV that is induced by the TPU process and the IR-induced ΔJ_p as a function of the bias voltage. When we choose a more negative bias voltage, we obtain a higher ΔV. The positive voltage change ΔV is explained by the adiabatic intraband excitation at the heterointerface of the TPU-SC; the accumulated electrons are transferred to the CB of the $Al_{0.3}Ga_{0.7}As$ barrier by absorbing IR photons and subsequently drifting due to the electric field at the interface. We also find that the onset bias voltages for ΔV and ΔJ_p are almost the same (near 0.8 V). The change in ΔV near the onset is gentler, which is consistent with the differences observed between the current-voltage curves

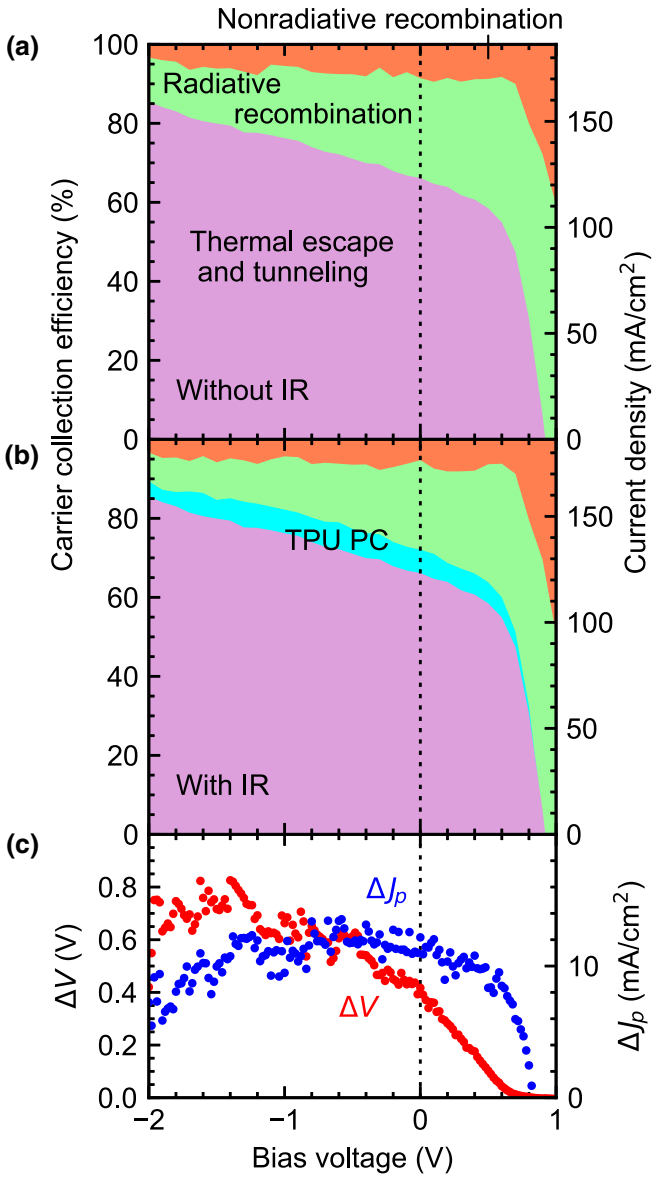

FIG. 5. (a),(b) Carrier collection efficiency of the TPU-SC (a) without and (b) with additional IR irradiation. The contributions of the different types of current loss and current extraction mechanisms are indicated by the colored areas. (c) Bias-voltage dependence of voltage increase ΔV caused by the additional IR irradiation, and of ΔJ_p.

measured with and without IR irradiation, as shown in our previous publication [24]. At strong reverse bias voltages, both ΔV and ΔJ_p start to decrease, because the electron density at the heterointerface decreases.

The excitation power densities of 0.70 W/cm^2 (for interband excitation) and 1.85 W/cm^2 (for intraband excitation) used in this experiment correspond to 17 and 84 suns, respectively. The fraction of the generated electrons accounted for by the short-circuit TPU PC, $\Delta J_p(0\ \mathrm{V})$, in Fig. 5(b) is 6.5% under these excitation conditions. In this experiment, the suns-equivalent value of the intraband excitation is stronger than that of the interband excitation. If both the suns-equivalent values are 17, the fraction corresponding to $\Delta J_p(0\ \mathrm{V})$ can be roughly estimated as 2.0% if the relationship between $\Delta J_p(0\ \mathrm{V})$ and the intraband excitation intensity $P_{\mathrm{ex,IR}}$, $\Delta J_p(0\ \mathrm{V}) \propto {P_{\mathrm{ex,IR}}}^{0.73}$ [see Fig. 7(b) of Ref. [24]], applies. Furthermore, if we use the data shown in Fig. 1(a) of Ref. [25], the fraction corresponding to $\Delta J_p(0\ \mathrm{V})$ under 1-sun illumination is expected to be 4.5%.

IV. CONCLUSION

We investigate carrier collection and recombination processes at the heterointerface in a TPU-SC. To characterize radiative recombination, the PL is integrated over the range from 1000 to 1300 nm. The magnitudes of the PC and PL signals generated via interband excitation of the GaAs layer depend on the bias voltage, and we confirm a reciprocal relation between the PC (corresponding to intraband transitions) and the PL (corresponding to interband transitions). Our data show that the PC density increases and the PL intensity decreases when the solar cell is illuminated with additional IR light. We find that nonradiative recombination becomes significant above bias voltages of 0.58 V. In addition, the IR-induced change in the PC (PL) exhibits a gentle peak (dip) around −0.6 V, because of the trade-off relationship between enhanced electron extraction after IR absorption at the interface and a decrease in the electron density at the interface due to tunneling at large reverse bias voltages. We also confirm that the IR-induced change in the PL is not affected by the hole density at the heterointerface. Finally, we quantitatively evaluate the fractions of the generated electrons that are extracted as photocurrent, are lost via radiative recombination, and are lost via nonradiative recombination. This enables an assessment of the TPU efficiency within the accuracy of the assumptions employed (that is, negligible nonradiative losses at −2 V). For a bias of −0.6 V, 7% of the photogenerated carriers in GaAs are collected via TPU.

ACKNOWLEDGMENTS

The authors would like to thank Professor Yoshitaka Okada of the University of Tokyo and Dr. Yasushi Shoji of The National Institute of Advanced Industrial Science and Technology (AIST) for device fabrication. This work was partially supported by the Japan Society for the Promotion of Science (JSPS) KAKENHI, Grants No. 18K18862, No. 18KK0145, No. 19H00768, and No. 18H05952.

[1] A. De Vos, Detailed balance limit of the efficiency of tandem solar cells, J. Phys. D: Appl. Phys. **13**, 839 (1980).

[2] N. Ekins-Daukes, Strained and strain-balanced quantum well devices for high-efficiency tandem solar cells, Sol. Energy Mater. Sol. Cells **68**, 71 (2001).

[3] R. T. Ross and A. J. Nozik, Efficiency of hot-carrier solar energy converters, J. Appl. Phys. **53**, 3813 (1982).

[4] M. A. Green, Third generation photovoltaics: Ultra-high conversion efficiency at low cost, Prog. Photovolt.: Res. Appl. **9**, 123 (2001).

[5] M. A. Green, K. Emery, Y. Hishikawa, W. Warta, E. D. Dunlop, D. H. Levi, and A. W. Y. Ho-Baillie, Solar cell efficiency tables (version 49), Prog. Photovolt.: Res. Appl. **25**, 3 (2017).

[6] Y. Okada, N. J. Ekins-Daukes, T. Kita, R. Tamaki, M. Yoshida, A. Pusch, O. Hess, C. C. Phillips, D. J. Farrell, K. Yoshida, N. Ahsan, Y. Shoji, T. Sogabe, and J.-F. Guillemoles, Intermediate band solar cells: Recent progress and future directions, Appl. Phys. Rev. **2**, 021302 (2015).

[7] R. Y. Lin, *Advanced Solar Power Technology-Multiple Junction Photovoltaics* (Springer Singapore, Singapore, 2020).

[8] L. C. Hirst and N. J. Ekins-Daukes, Fundamental losses in solar cells, Prog. Photovolt.: Res. Appl. **19**, 286 (2011).

[9] W. Shockley and H. J. Queisser, Detailed balance limit of efficiency of p-n junction solar cells, J. Appl. Phys. **32**, 510 (1961).

[10] T. Kita, Y. Harada, and S. Asahi, *Energy Conversion Efficiency of Solar Cells* (Springer Singapore, Singapore, 2019).

[11] A. Luque and A. Martí, Increasing the Efficiency of Ideal Solar Cells by Photon Induced Transitions at Intermediate Levels, Phys. Rev. Lett. **78**, 5014 (1997).

[12] M. Yoshida, N. J. Ekins-Daukes, D. J. Farrell, and C. C. Phillips, Photon ratchet intermediate band solar cells, Appl. Phys. Lett. **100**, 3 (2012).

[13] Y. Shoji, R. Tamaki, and Y. Okada, Multi-stacked GaSb/GaAs type-II quantum nanostructures for application to intermediate band solar cells, AIP Adv. **7**, 065305 (2017).

[14] T. Tayagaki and T. Sugaya, Type-II InP quantum dots in wide-bandgap InGaP host for intermediate-band solar cells, Appl. Phys. Lett. **108**, 1 (2016).

[15] J. Hwang, K. Lee, A. Teran, S. Forrest, J. D. Phillips, A. J. Martin, and J. Millunchick, Multiphoton Sub-Band-Gap Photoconductivity and Critical Transition Temperature in Type-II GaSb Quantum-Dot Intermediate-Band Solar Cells, Phys. Rev. Appl. **1**, 1 (2014).

[16] S. Tomić, Effect of Sb induced type II alignment on dynamical processes in InAs/GaAs/GaAsSb quantum dots: Implication to solar cell design, Appl. Phys. Lett. **103**, 072112 (2013).

[17] E. Antolín, A. Martí, J. Olea, D. Pastor, G. González-Díaz, I. Mártil, and A. Luque, Lifetime recovery in ultra-highly titanium-doped silicon for the implementation of an intermediate band material, Appl. Phys. Lett. **94**, 042115 (2009).

[18] A. Takahashi, T. Ueda, Y. Bessho, Y. Harada, T. Kita, E. Taguchi, and H. Yasuda, One-dimensional miniband formation in closely stacked InAs/GaAs quantum dots, Phys. Rev. B **87**, 235323 (2013).

[19] T. Kaizu, T. Matsumura, and T. Kita, Broadband control of emission wavelength of InAs/GaAs quantum dots by GaAs capping temperature, J. Appl. Phys. **118**, 154301 (2015).

[20] K. Yamaguchi and T. Kanto, Self-assembled InAs quantum dots on GaSb/GaAs(001) layers by molecular beam epitaxy, J. Cryst. Growth **275**, e2269 (2005).

[21] A. Luque, A. Martí, and C. Stanley, Understanding intermediate-band solar cells, Nat. Photonics **6**, 146 (2012).

[22] W. G. Hu, T. Inoue, O. Kojima, and T. Kita, Effects of absorption coefficients and intermediate-band filling in InAs/GaAs quantum dot solar cells, Appl. Phys. Lett. **97**, 193106 (2010).

[23] S. Asahi, H. Teranishi, N. Kasamatsu, T. Kada, T. Kaizu, and T. Kita, Saturable Two-step photocurrent generation in intermediate-band solar cells including InAs quantum dots embedded in $Al_{0.3}Ga_{0.7}$/GaAs quantum wells, IEEE J. Photovolt. **6**, 465 (2016).

[24] S. Asahi, H. Teranishi, K. Kusaki, T. Kaizu, and T. Kita, Two-step photon up-conversion solar cells, Nat. Commun. **8**, 14962 (2017).

[25] S. Asahi and T. Kita, Reply to: "thermal artefacts in two-photon solar cell experiments,", Nat. Commun. **10**, 956 (2019).

[26] S. Asahi, K. Kusaki, Y. Harada, and T. Kita, Increasing conversion efficiency of two-step photon up-conversion solar cell with a voltage booster hetero-interface, Sci. Rep. **8**, 872 (2018).

[27] M. L. Bimberg and D. Grundmann, in *Quantum Dot Heterostructures*, (John Wiley & Sons, New York, 1998).

[28] P. Harrison, *Quantum Wells, Wires and Dots* (John Wiley & Sons, Ltd, Chichester, UK, 2005).

[29] S. Birner, T. Zibold, T. Andlauer, T. Kubis, M. Sabathil, A. Trellakis, and P. Vogl, Nextnano: General purpose 3-D simulations, IEEE Trans. Electron Devices **54**, 2137 (2007).

[30] U. Rau, Reciprocity relation between photovoltaic quantum efficiency and electroluminescent emission of solar cells, Physical Review B **76**, 085303 (2007).

[31] T. Kirchartz and U. Rau, Detailed balance and reciprocity in solar cells, Phys. Status Solidi (A): Appl. Mater. Sci. **205**, 2737 (2008).

[32] T. Kirchartz, A. Helbig, W. Reetz, M. Reuter, J. H. Werner, and U. Rau, Reciprocity between electroluminescence and quantum efficiency used for the characterization of silicon solar cells, Prog. Photovolt.: Res. Appl. **17**, 394 (2009).

[33] K. Toprasertpong, A. Delamarre, Y. Nakano, J. F. Guillemoles, and M. Sugiyama, Generalized Reciprocity Relations in Solar Cells with Voltage-Dependent Carrier Collection: Application to p - I - n Junction Devices, Phys. Rev. Appl. **11**, 1 (2019).

[34] T. Kirchartz, A. Helbig, and U. Rau, Note on the interpretation of electroluminescence images using their spectral information, Sol. Energy Mater. Sol. Cells **92**, 1621 (2008).

[35] U. Aeberhard and U. Rau, Microscopic Perspective on Photovoltaic Reciprocity in Ultrathin Solar Cells, Phys. Rev. Lett. **118**, 247702 (2017).

[36] S. Asahi, T. Kaizu, and T. Kita, Adiabatic two-step photoexcitation effects in intermediate-band solar cells with quantum dot-in-well structure, Sci. Rep. **9**, 7859 (2019).